Journal of Power Sources 266 (2014) 512–519

Contents lists available at ScienceDirect

Journal of Power Sources

journal homepage: www.elsevier.com/locate/jpowsour

State-of-health monitoring of 18650 4S packs with a single-point impedance diagnostic

Corey T. Love [a,*], Maheboob B.V. Virji [b], Richard E. Rocheleau [b], Karen E. Swider-Lyons [a]

[a] Chemistry Division, U.S. Naval Research Laboratory, Washington, DC 20375, USA
[b] Hawaii Natural Energy Institute, University of Hawaii at Manoa, Honolulu, HI 96822, USA

HIGHLIGHTS

- A single-point impedance method tracks the state-of-health (SOH) of Li-ion batteries.
- The impedance response at 316 Hz is reflective of the SOH for a commercial 18650 cell.
- The SOH of single 18650 cells and 4S packs are monitored during overcharge.
- The overcharge abuse of a single cell is detected within a 4S battery pack.
- The single-point impedance diagnostic works on packs without single-cell monitoring.

ARTICLE INFO

Article history:
Received 31 March 2014
Received in revised form
8 May 2014
Accepted 9 May 2014
Available online 20 May 2014

Keywords:
Electrochemical impedance spectroscopy
Lithium ion battery
State of health
Overcharge
Safety
18650

ABSTRACT

The state-of-health (SOH) of Li-ion batteries and battery packs must be monitored effectively for abuse to prevent failure and accidents. In a previous publication, we described a single-point impedance diagnostic method for detecting damage in single prismatic lithium polymer rechargeable cells subjected to overcharge abuse. We now determine whether the single-point impedance diagnostic method is applicable to 4S battery packs. At 316 Hz, commercial 18650 $LiCoO_2$ cells are determined to have the least change in impedance response when cycled between 3.0 and 4.2 V, for states-of-charge (SOC) of 0–100%. The impedance response of single cells at 316 Hz changes dramatically during overcharge (SOC = 125%), presumably due to change in their solid electrolyte interface (SEI) layers at the electrodes. When a single cell is purposely subjected to such overcharge abuse and then integrated into a 4S pack with 3 other healthy cells, the impedance response of the 4S pack at 316 Hz also changes, despite variances in the impedance response of each of the 3 healthy cells. The results suggest that this single-point impedance method could serve as a diagnostic in an all-inclusive battery management system to identify overcharge abuse of single cells without individual cell monitoring.

Published by Elsevier B.V.

1. Introduction

Lithium-ion or lithium-polymer batteries (LiBs) are becoming the ubiquitous power sources for consumer electronics, and large packs are now being used in hybrid-electric and electric vehicles (HEVs and EVs) [1]. The features that makes LiBs attractive—their high specific energy and energy density—also make them subject to ignition, particularly because the fuel (lithium) and oxidizer (cathode) are encapsulated in each cell in close contact in the midst of a flammable organic electrolyte. Catastrophic failures of LiBs have resulted in fires in laptops, automobiles and airplanes. The failures likely start within single cells having manufacturing defects and/or from improper charging practices.

Cells connected in series are more susceptible to failure due to irregularity in load (charge and voltage) leveling. For the case of cells connected in series (as is presented in this work) each cell will experience the same current when the pack is charged or discharged however cell voltages may deviate from one another during the process. An unbalanced battery pack may exhibit a “normal” pack voltage reading while the constituent cells rest at different voltages or states of charge (SOC). Inaccurate SOC determination can lead to overdischarge or overcharge causing instability within the battery [1] which can lead to catastrophic failure in the form of thermal runaway [2,3].

In order to operate LiBs effectively, basic research is being done to understand the failure mechanisms, but controls for battery

* Corresponding author. Tel.: +1 202 404 6291.
E-mail address: corey.love@nrl.navy.mil (C.T. Love).

http://dx.doi.org/10.1016/j.jpowsour.2014.05.033
0378-7753/Published by Elsevier B.V.

management systems (BMSs) must also be developed to recognize when a LiB is in poor state-of-health (SOH) and its operation should be ceased. SOH diagnostic methods should be incorporated in a comprehensive BMS which is sensitive to faults in a single cell within a battery pack, as the failure of a lone cell can initiate cascading failures of neighboring cells. The diagnostics are ideally carried out on cell packs and not individual cells to minimize wiring and data collection. Other desired attributes of a BMS are the ability to manage continuous and regenerative charging, monitor and maintain safe levels of charge and diagnose problems within a battery.

Impedance-based diagnostic techniques are likely components of any BMS since resistance is a function of the key indicators of battery health. Impedance-based methods to measure internal cell temperature have been reported by Srinivasan et al., who monitored phase shift changes with temperature [4] and attributed to anode entropy [5], and recently by Schmidt via measurement of the real impedance response at high frequency [6]. These reports show little dependence of real impedance and phase angle (Z', θ) with SOC at a single frequency. Dubarry et al. have developed predictive models for battery performance under a variety of duty cycle regimes [7]. Even with previous history information, current prognostic models do not account for secondary, intermediate or parasitic reactions occurring within the cell [7]. Electrochemical impedance spectroscopy (EIS) measurements based upon laboratory derived equivalent circuits models require signal generation, data acquisition and processing hardware to perform the necessary voltage or current amplitude applied over a full sweep of frequencies, 10^6–10^{-3} Hz leading to expensive electronics and long data analysis times [8,9]. Also, equivalent circuits models needed for decision-making require distributed or nonlinear elements such as the Warburg impedance making onboard real-time application problematic [2].

In a previous publication we showed the opportunity for a single-point impedance diagnostic for monitoring overcharge abuse and the overall SOH of 30 mAh lithium-polymer prismatic cells [10]. We found that the impedance response of the cell at 500 Hz was largely invariant within its normal operating range (0–100% SOC). Once the battery was overcharged, its impedance at 500 Hz first decreased significantly, and then increased in subsequent cycles, presumably due to changes in the resistance of the electrode passivation layers or solid electrolyte interface (SEI). Specifically, the impedance associated with SEI is invariant within the normal operating range, 0–100% SOC but after a single overcharge event the capacitive and resistive natures of the SEI layers are altered which produces a less negative imaginary impedance (Z'') followed by a shift towards higher and higher real impedance (Z'). We concluded that 500 Hz could be used as a "state-of-health frequency" or f_{SOH}, to adeptly monitor the electrochemical processes in the cell, and that it was not necessary to monitor a wide range of frequencies, thereby simplifying the diagnostic.

The single-point impedance method is effective because it is sensitive to the SEI, and the SEI is key to battery safety. Once the SEI forms on the surface of the negative and positive electrodes from the electrolyte in contact with the electrodes, it provides passivation to protect against further electrolyte decomposition occurring at the electrode/electrolyte interfaces [11]. Discontinuous or ruptured SEI layers will not protect against electrolyte oxidation/reduction, leading to lithium depletion and increasing cell resistance which can severely limit a cell's remaining useful life or in the worst-case initiate the thermal runway reaction [12,13] leading to catastrophic failure. Mass and charge transport limitations through the thickness of the SEI also contribute to the resistance. The impedance associated with the SEI layers is in the high-to-mid frequency range (1000–100 Hz) of the electrochemical impedance spectrum for LiBs, or on the order of milliseconds [14–20] in the time domain. The resistance in this range has been associated with the SEI, typically on the anode, via deconvolution of the Nyquist plot through implementation of an equivalent circuit model.

Abuse to a lithium-ion battery by overcharge, overdischarge or thermal abuse irreversibly affects the SEI impedance. Therefore, monitoring the impedance in the range where the SEI responds provides useful information into the efficiency of electrochemical processes and a general measure of the cell's SOH is rational. However, individual cells are also expected to show impedance variation due to slight differences in manufacturing and cell interconnects add additional resistance and inductance. When cells are wired in series, such changes in resistances are additive. The question remains whether the f_{SOH} for a single cell translates across multiple cells, and how sensitive it is to changes in the SOH of single unhealthy cells within a battery pack.

In this paper, we expand our prior measurements of a single lithium-polymer cell [10], to packs of four 18650 $LiCO_2$ cells in series to determine whether the methodology is applicable across systems and whether it must be applied to individual cells or can be used at the pack level. We first determine the f_{SOH} from the frequency at which the impedance response of individual $LiCoO_2$ cells has the least variance over their normal operating SOC from 0 to 100%, and then confirm that the impedance of the cell at this f_{SOH} changes with overcharge abuse. 4S packs of the $LiCO_2$ cells are constructed, and then the same determination of the f_{SOH} is made on the pack. Finally, we insert a single cell subjected to overcharge abuse into a 4S pack with 3 other healthy cells and determine whether it can be detected. We also implement a new impedance tool called the FlexiMIST (Flexible Signal Multichannel Impedance Spectrometry Tool) to measure the 4 cells individually whilst monitoring the pack impedance.

2. Experimental

2.1. Testing single cells

Cylindrical 18650 lithium-ion rechargeable cells (Tenergy Battery Corp., Fremont, CA) of $LiCoO_2$|C chemistry were tested in this work as individual cells and as part of a pack of 4 cells in series (4S). The nominal cell voltage and capacity are 3.7 V and 2.6 Ah, respectively. The manufacturer recommended charge/discharge voltage boundaries are between 3.0 and 4.2 V. Printed safety circuit boards were removed from the cells prior to testing.

Galvanostatic cycling was performed within the manufacturer specified voltage range of 3.0–4.2 V unless otherwise noted. The upper voltage boundary was increased to 4.6 V for the overcharge (OC) condition. Electrochemical impedance of single cells was measured at various SOCs between 50 kHz–10 mHz by applying a voltage perturbation of 40 mV. To test the versatility and repeatability of the single-point impedance technique, three different impedance instruments were used in this study. The characteristic features of each are given in Table 1. Impedance measurements of individual cells were tested using the Solartron 1260, Maccor Frequency Response Analyzer 0356 (FRA) and the FlexiMIST developed at the Hawaii Natural Energy Institute (HNEI) and Grandalytics, Inc.

The typical protocol for EIS data collection at various SOC for single cells (corresponding to Fig. 4) was:

1. Constant current (CC) charge to 4.2 V at 1.3 A (C/2)
2. Constant voltage (CV) charge at 4.2 V until $I < .02$ A
3. Rest 10 min under open circuit condition
4. Collect electrochemical impedance spectra; 50 kHz–10 mHz at 40 mV amplitude

Table 1
EIS experiments from 50 kHz to 10 mHz.

Impedance instrument	Test item	Function
Solartron 1260	Single Cells	• identify f_{SOH}
Maccor FRA 0356	Single Cells	• identify f_{SOH}
FlexiMIST	Single Cells	• validation of f_{SOH} from Solartron & Maccor
FlexiMIST	4S Pack	• pack impedance • validation of f_{SOH} in 4S configuration

5. CC discharge to 4.0 V at 1.3 A (C/2)
6. Rest 10 min under open circuit condition
7. Collect electrochemical impedance spectra; 50 kHz–10 mHz at 40 mV amplitude
8. Repeat steps 5–7 decreasing the cut-off voltage by 100 mV until reaching 3.0 V
9. Reverse the process by collecting impedance spectra every 100–200 mV during 1.3 A CC charge steps

The typical protocol for EIS data collection at before, during and after overcharge (OC) for single cells (corresponding to Fig. 6) was:

1. Constant current (CC) charge to 4.2 V at 1.3 A (C/2)
2. Constant voltage (CV) charge at 4.2 V until $I < .02$ A
3. Rest 10 min under open circuit condition
4. Collect electrochemical impedance spectra, **Initial**; 50 kHz–10 mHz at 40 mV amplitude
5. CC overcharge to 4.6 V at 1.3 A (C/2)
6. Rest 10 m under open circuit condition
7. Collect electrochemical impedance spectra, **OC1**; 50 kHz–10 mHz at 40 mV amplitude
8. CC discharge to 4.0 V at 1.3 A (C/2)
9. Rest 10 min under open circuit condition
10. Collect electrochemical impedance spectra; 50 kHz–10 mHz at 40 mV amplitude
11. Repeat steps 5–10 4*x* to obtain successive overcharges **(OC2-OC5)** and return to 4.2 V **(2–5)**

2.2. Fabrication and testing of the 4S pack

Battery packs composed of four 18650 single cells in series (4S) were fabricated to yielded a nominal pack voltage and capacity of 14.8 V and 2.6 Ah, respectively. The positive part of the printed circuit board (PCB) tabs of each cell, acting as positive (+) terminal, were used to connect the four cells in series. Thick (16 AWG) cables were used at both ends of the 4S pack for charging and discharging of the battery pack, while the thin (24 AWG) cables were implanted on each cell while and connected to a 9-pin Sub-D connector to interface with the FlexiMIST for impedance measurements. The Cell 1 (+) and Cell 4 (−) were the positive and negative terminals of the pack. Each cell-to-cell connection was properly insulated to avoid shorting between cells. The battery pack was wrapped in heat sink for safety purposes and folded to make it compact to minimize wiring inductance. Fig. 1 shows the pictures of the fabrication process for the four single cells to a fully instrumented 4S pack to a compact battery pack implemented in a safety enclosure for testing.

The FlexiMIST provided impedance measurements of the individual cells within the 4S pack as well as the entire pack itself. FlexiMIST is a data acquisition system with the capability of measuring fast and simultaneously high frequency impedance of all individual cells of the battery pack. The FlexiMIST system is modular and scalable to the desired number of cells. The HNEI FlexiMIST system had three carrier cards with 8 channels of isolated, simultaneously sampling digitizers each and a total of 24 plug-in signal conditioning modules. These modules included 9 DC and 9 AC coupled voltage channels, and 6 RTD temperature channels for measurement of cell voltage, shunt voltage and temperature.

Fig. 2 shows the HNEI battery test-bed schematic with implementation of the FlexiMIST system, the 4S battery pack, 4-quadrant power amplifier and National Instrument PX1 controller. The test-bed has frequency, voltage and current range of: 10 mHz–100 kHz, ±20 V and ±16 A respectively. The customized software analyzed the measured data to determine the impedance of the 4S battery pack as well as each individual cell.

The protocol for EIS data collection using FlexiMIST at various SOC and for single cells within the 4S pack as well as the overall pack impedance was identical to the procedure outlined above for single cells. During the overcharge experiment to the 4S pack, only Cell 2 was overcharged using CC of 1.3 A to a cutoff voltage of 4.6 V and 4.75 V. After the rest periods following Cell 2 overcharge the cell voltages relaxed to 4.52 and 4.62 V, respectively. Because the impedance was collected while Cell 2 was in the relaxed state, we refer to these values for cell voltage throughout the paper as opposed to the upper voltage cutoff voltages.

2.3. Impedance data analysis

Impedance data were analyzed to determine the frequency that showed the smallest statistical variation with SOC (0–100%). The

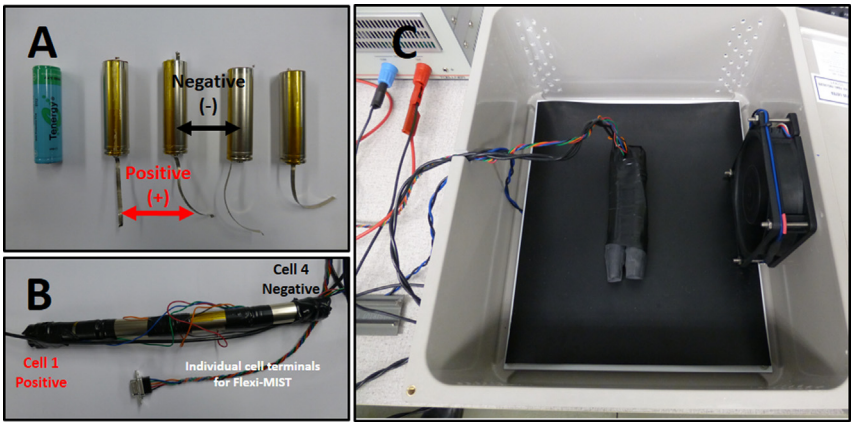

Fig. 1. Fabrication process of 18650 cells into a 4S pack: (A) initial 18650 cell and 4 cells with external PCBs removed, (B) wiring four cells in series, and (C) 4S pack in safety enclosure before test.

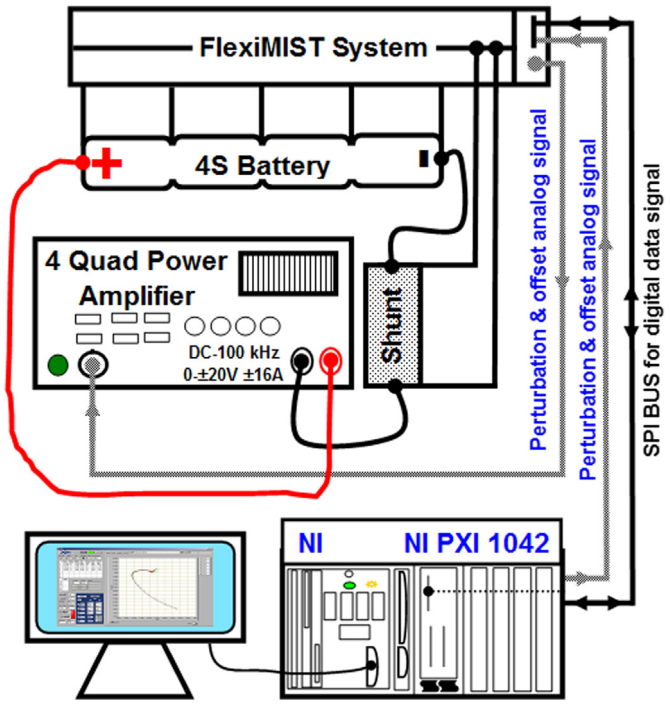

Fig. 2. Schematic representation of HNEI battery test-bed.

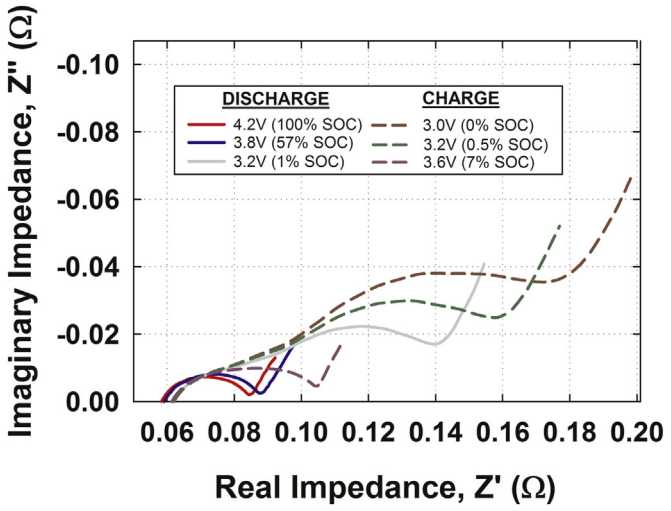

Fig. 3. Impedance spectra collected at various SOC of a 18650 cell during typical discharge/charge between 3.0 and 4.2 V (0–100% SOC).

average impedance values (Z′ and Z″) along with the standard deviation ($\pm\sigma_{Z'}$ and $\pm\sigma_{Z''}$) at discrete frequencies over the full range of SOC were calculated using traditional data analysis and plotting software (Excel and SigmaPlot).

3. Results

3.1. Determination of the SOH frequency

Lithium-ion cells produce different impedance responses with changes in cell voltage and SOC. The Nyquist plot in Fig. 3 shows changes in both the shape and magnitude in the real vs. imaginary impedance curve of a single 18650 cell during a typical cell discharge/charge cycle between 3.0 and 4.2 V, or 0–100% SOC, respectively. At 100% SOC, the impedance response forms a small single arc with impedance of nearly 20 mΩ. The single arc contains impedance contributions from both the negative and positive electrodes although dominated by the cathode effects. As the SOC decreases to 3.8 V (57% SOC) a second arc emerges in the mid-to-low frequency region and grows ultimately until the cut-off voltage is reached at 3.0 V (0% SOC). The second arc decreases upon charging and returning to the fully charged state. The low frequency arc is assigned to charge transfer resistance and impedance due to ionic diffusion within the porous electrodes. No change in the impedance spectra is observed at 4.2 V before and after the discharge/charge cycle as both curves lie on top of one another.

As shown in Fig. 3, there is little deviation in the impedance response of a representative 18650 cell from 0 to 100% SOC in the high frequency inductance region ($Z'' > 0$) and in the initial portion of the high frequency arc. The standard deviation in impedance with SOC is shown in Fig. 4A. The red line (in the web version) in Fig. 4A shows the average impedance measured over all the SOCs (charge and discharge) given in Fig. 3 plus at additional voltages, and the error bars represent the standard deviation of the impedance responses measured at each specific frequency. When the standard deviation at a certain frequency is small, the impedance response can be thought to be nearly independent of SOC. Fig. 4A inset is expanded to Fig. 4B to identify three frequencies that exhibit the smallest deviation in impedance with SOC: 500 Hz, 316 Hz and 100 Hz. At 316 Hz, Z′ of this battery is 0619 ± .0016 (or ±2.5%), and Z″ is −.0023 ± .0001. The observed deviations are almost entirely due to changes in Z′ likely due to changes in the $LiCoO_2$ resistance with SOC. Regardless, no noticeable changes are observed in the imaginary impedance at these frequencies when discharged/charged within the recommended voltage window of 3.0–4.2 V.

The single-point SOH frequency for the Tenergy 18650 cells is determined to be ~316 Hz as determined by Fig. 4B and Figure S1 where the standard deviation of the real impedance with SOC, $\sigma_{Z'}$, reaches a minimum while the standard deviation of the imaginary impedance, $\sigma_{Z''}$, is nearly constant. The SOH frequency corresponds to the time constant according to the relationship, $\tau = f^{-1}$. The lower the time constant, the faster the current changes at fast voltage changes. The 40 mV sinusoidal perturbation in this work correlates for a time constant of $\tau \approx .5$ ms. The time constant will change as a function of the surface chemistry of the cell electrodes [21] and possibly even the cell geometry [22]. In the frequency range 500–100 Hz the imaginary impedance is nearly constant with frequency.

While the variations in impedance with SOC are lowest at the 316 Hz SOH frequency, an acceptable range of dispersion from the arithmetic mean is determined as a pass or fail grade of the response to the single-point perturbation. Fig. 4C shows the spread of impedance values at the 316 Hz SOH frequency at various SOCs. Three factors (1σ, 2σ, 3σ) of the standard deviation originating from the average Z′, Z″ impedance over all SOCs are drawn where 1σ is the deviation measured for 1 cell, and the factors of 2σ and 3σ represent scaling of the data by a factor of 2× and 3× respectively. All of the data collected within the normal operating voltage (3.0–4.2 V) lay within 2*x* the standard deviation or 2σ. For purposes of this paper, these variances in the standard deviation are used to approximate the acceptable limits of impedance variation attributed to battery SOH information. More robust accounting of the variation in impedance response with SOC could be achieved

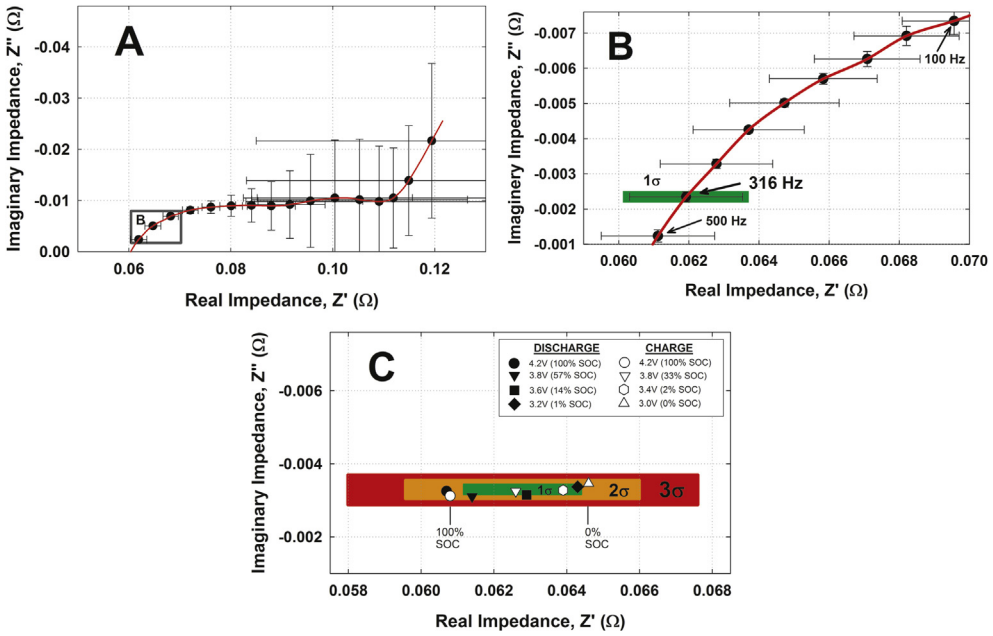

Fig. 4. (A) Mean impedance values and standard deviations for all SOCs. For clarity the black circles represent every 3rd data point. (B) Expand Fig. 4A inset to show all frequencies collected between 500 and 100 Hz. (C) SOH chart illustrating the change in impedance response collected at 316 Hz perturbation frequency with SOC. Deviation from the average impedance is shown by the increasing factors of deviation: 1, 2 and 3*x* the standard deviation (1σ, 2σ, 3σ) with SOC.

through use of common statistical analysis measures of variance, mean difference, etc.

A general trend in Fig. 4C shows the effect of SOC on Z′ and Z″. As the cell is discharged the real impedance increases while the imaginary impedance decreases towards more negative values ($f_{SOH} = 316$ Hz). The reverse trend is true upon subsequent charging where Z′ decreases and Z″ becomes less negative. Slight variations near the $Z'' = 0$ intercept may be indicative of variances in the cell and connector inductance. The decrease in real impedance during the charging process can be ascribed to a decrease in the materials resistance. Likewise the decrease in imaginary impedance during the charge process shows the increased conductivity of Li^+ ion saturated solid electrolyte interface on the anode which could be reduced to metallic lithium [23]. The largest variation in impedance taken at 200 mV cell voltage intervals are between the largest gaps in cell SOC; 57–14% during discharge while 78–33% and 33–7% are nearly equidistant during charge (not all data points shown for clarity). Previous work by Zhang and Jow has shown the resistance associated with the bulk (electrolyte, separator, electrodes) and SEI remain unchanged for commercial electrodes cycled between 3.2 and 4.2 V [11,24]. Additionally, Nelson et al. observed only modest impedance change within the middle SOC range [25], approximately 25–75% SOC.

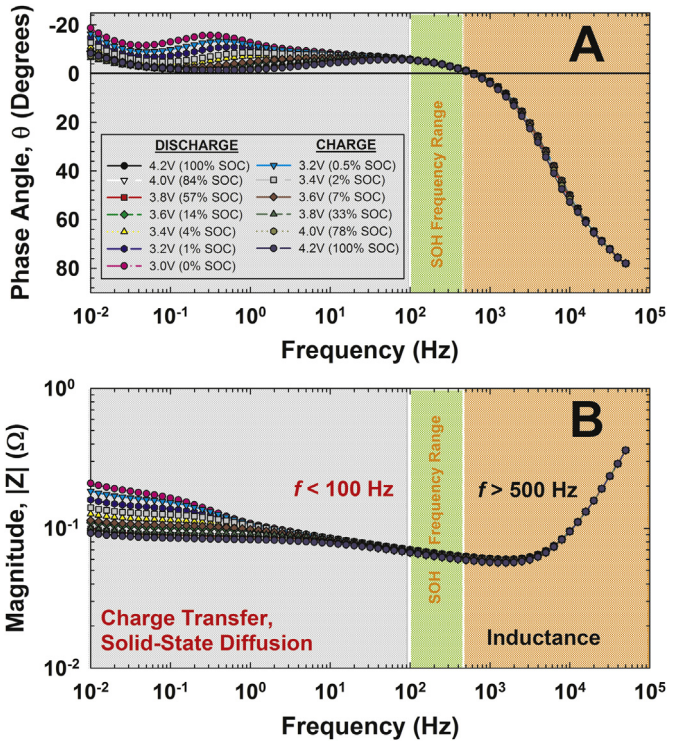

Fig. 5. (A) Phase angle and (B) magnitude of impedance as a function of frequency for data collected between 0 and 100% SOC during discharge and charge. The SOH frequency region is highlighted in green where the impedance originated from electrochemical processes is nearly independent of SOC. (For interpretation of the references to color in this figure legend, the reader is referred to the web version of this article.)

To separate the contributions of resistance, capacitance and inductance, the phase angle and impedance magnitude versus frequency are shown 500–100 Hz in, Fig. 5A and Fig. 5B, respectively. To minimize the effects of inductance from non-chemical factors (fabrication and connectors), we negate frequencies which produce a positive phase angle, θ. Therefore, the intercept at $\theta > 0$ serves as the SOH frequency high boundary. The magnitude of impedance is the magnitude of the impedance vector with contributions from the real and imaginary components, such that:

$$|Z| = \sqrt{Z'^2 + Z''^2} \quad [1]$$

Low frequency impedance changes are due to fluctuations in the concentration of Li^+ within the positive and negative electrodes. During charge and discharge approximately .5 mol Li^+ shuttles between the electrodes [26] accounting for changes in solid-state-diffusion and charge transfer resistance [27]. Since the impedance magnitude accounts for fluctuations in both the real and imaginary

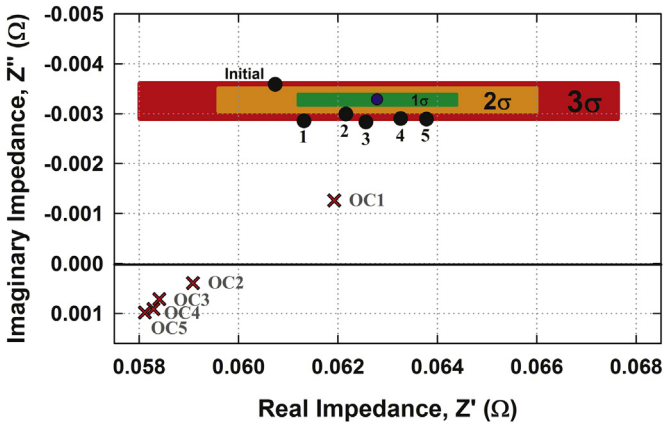

Fig. 6. SOH chart illustrating the average impedance value at the 316 Hz SOH frequency (blue circle) encircled by the ±1, 2 and 3x standard deviation (1σ, 2σ, 3σ) as determined in Fig. 4C. The impedance response of the cell at 4.56 V (125% SOC) overcharge (OC) and subsequent discharge to 4.2 V (100% SOC) represented by black circles for repeated overcharges, 1 through 5 represented by red "X" marks. (For interpretation of the references to color in this figure legend, the reader is referred to the web version of this article).

components, frequency regions of Fig. 5B with little deviation with SOC are ideal for the SOH frequency. Separation of the impedance magnitudes begins below 100 Hz. The least deviation in impedance response with all SOCs is given between 500 and 100 Hz.

3.2. Detection of overcharge abuse in single cells

The utility of the diagnostic is to identify cell abuse before a serious malfunction, failure or catastrophic event. Single Tenergy 18650 cells were mildly overcharged to 4.56 V (125% SOC) for 5 consecutive cycles. The impedance responses to overcharge at the SOH frequency is shown in Fig. 6 against the average impedance and variance from 4 cells to give the 1σ, 2σ, and 3σ boundaries. The initial impedance at full SOC lies within the 3σ boundary previously determined by another cell. As expected the real impedance value is nearly identical to that shown in Fig. 4C (4.2 V, 100% SOC). However there is a slight shift towards more negative imaginary impedance in Fig. 6. A period of 2 weeks separated the end of the initial experiments in Fig. 4 and the beginning of the experiment shown in Fig. 6. All external factors such as the cell connections and instrument leads were left unchanged during this time period suggesting the decreased imaginary resistance is due to an aging effect within the cell. Invariance in the real impedance also suggests external factors do not contribute to this change. When taking the effects of aging into account, the SOH range must be expanded to the 3σ boundaries. The impedance collected at the first overcharge condition (4.56 V) is designated by **OC1**. At the overcharge condition of **OC1** (125% SOC) both Z′ and Z″ increase. After **OC1** the cell was returned to 4.2 V to compare the initial impedance. There is a small shift in the real and imaginary impedance towards more positive values when the cell is returned to 4.2 V (point "**1**"). The impedance collected at repeated OC conditions shifts towards lower Z′ and change to positive Z″ during **OC2** through **OC5**. Each subsequent OC cycle increases the real impedance when the cell is returned to 4.2 V showing a trend towards higher real impedance. The impedance collected at excessive charge voltages deviates further towards lower Z′ and higher Z″.

3.3. Expansion from single cells to the 4S pack

To test the applicability of the single-point impedance method to more realistic battery packs, four Tenergy 18650 cells were wired in series (4S) to form battery packs. Impedance data was collected though the FlexiMIST explained in the experimental section. The impedance of each individual cell was monitored as well as the overall pack impedance with SOC. The average impedance for each cell within the 4S pack with SOC along with error bars indicating ±1σ as given in Fig. 7 during discharge (Fig. 7A–D) and charge (Figure S2A–D). Fig. 7E shows the overall 4S pack impedance along with the summation of individual cell impedances for Cells 1–4 during discharge, Σ(Cells 1–4). Specific impedance values at 100, 316 and 500 Hz are listed in Table S1. A good correlation exists between the pack impedance and the series impedance indicating good wiring of the 4S pack. Like voltage, resistance is summed when cells are wired in series as shown in Figure S2E where the summation of individual cell impedances within the pack is nearly identical to the impedance of the whole 4S pack. The impedance response of Cells 1, 2 and 4 are nearly identical and representative of the Tenergy 18650 cells. Cells 3 in the 4S pack however varies significantly especially at low frequency. Impedance testing over a large lot of individual cells shows similar variability on the order of 1 cell in every 4 or 5 likely the

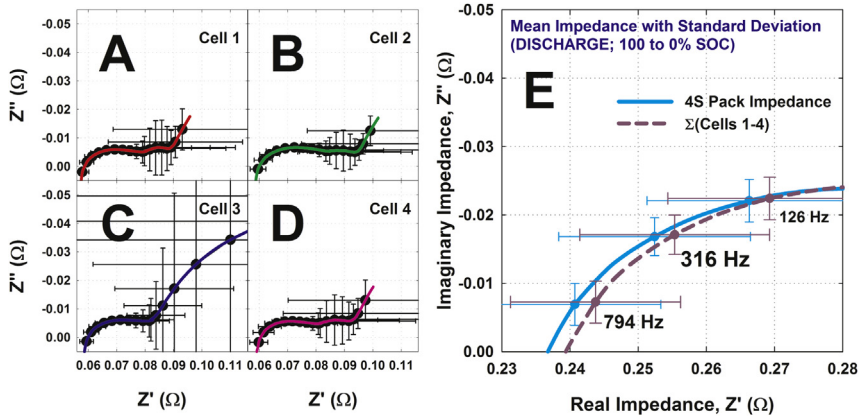

Fig. 7. (A–D) Impedance spectra for individual cells within 4S pack during discharge from 100 to 0% SOC. The average impedance value is given by the solid lines (red, green, blue and pink). The error bars indicate the standard deviation from the average impedance value at various SOC from 100 to 0%. (E) The light blue solid line shows the mean impedance with for the 4S pack at various SOCs during discharge. The dashed purple line is the summation of the impedance values from each of the individual cells given in A through D. The error bars indicate standard deviation from the average or summation impedances. For clarity every 4th data point (with error bars) is shown by a black circle symbol. (For interpretation of the references to color in this figure legend, the reader is referred to the web version of this article).

Table 2
Cell voltages (in Volts) during overcharge regime illustrated in Fig. 8.

Cell/stage	I	II	III	IV	V	$\Delta V = V_V - V_I$
Cell 1	4.17	4.15	4.17	4.16	4.17	0
Cell 2	4.17	4.52	4.18	4.62	4.19	+0.02
Cell 3	4.10	4.09	4.10	4.08	4.08	−0.02
Cell 4	4.16	4.14	4.16	4.15	4.16	0

result of variability in manufacturing, production date, storage time or shipping conditions.

Some cell imbalance was observed in the 4S pack in the fully charged state. Table 2 lists the individual cell voltages of the cells within the 4S pack before, during and after overcharge regime given in Fig. 8. Cell 3 voltage was lowest of the four cells where there was a 70 mV voltage difference between the highest voltages and lowest voltage cells. As Cell 2 is overcharged to 4.52 V (Fig. 8II) each of the surrounding cells decreases in voltage by 20 mV. After the initial overcharge, Cell 2 is discharged back to 4.2 V (Fig. 8III). Only a modest increase of 10 mV is observed for Cell 2 after overcharge. The increase in Cell 2 voltage continues after the overcharge to 4.62 V. The overall net voltage increase for Cell 2 is +20 mV while most of the voltage is compensated by the further weakening of Cell 3 (−20 mV). Overcharge of a single cell causes imbalance within the pack further weakening the inferior cells [28]. As the overcharged cell increases and the weaker cells decrease, the voltage differential grows creating more charge imbalance and fluctuations in pack voltage.

The single-point impedance diagnostic was employed to monitor the impedance response of the individual cells and the 4S pack impedance before and after overcharges to Cell 2. Fig. 9A shows the tight grouping of impedance values for Cells 1, 3 and 4 all fall within the ±2σ SOH region as determined from the data compiled for the 4S during database development. The overcharged cell, Cell 2, shows the largest variation in impedance. Modest overcharge of Cell 2–(4.52 V) causes a shift towards less negative imaginary impedance as shown previously for the single cells tested by the Solartron. The impedance response collected at 4.62 V deviates outside of the 3σ SOH range, clearly indicating abuse to the pack. However, after the subsequent discharge to the normal voltage ~4.2 V the impedance is recovered to within the 2σ region. The large variation in Cell 2 impedance at 4.6 V is also clearly seen in the 4S pack impedance in Fig. 9B. The pack impedance at 17.01 V pack voltage enters into the 3σ SOH region. Since the SOH region of the pack includes the summation of deviation from the individual cells, it provides a more conservation estimation of error within the impedance measurements. Therefore, the pack impedance SOH region could be taken as 1σ clearly identifying a problem encountered within the pack after the 4.62 V overcharge to Cell 2.

3.4. Correlation of impedance across multiple instruments

The average impedance and standard deviation over the full range of SOC for each instrument are given in Table 3 and compared to the average impedance with SOC and variance of individual cells collected by the Solartron and FlexiMIST.

The results for the 4S packs are, as expected, additive of the performance of the single cells. The measured deviation in the impedance of a single abused cell within the 4S pack is sufficient to push the impedance outside the expected impedance range. In Fig. 9B, the impedance of the healthy cells are about 10× different from when there is an unhealthy cell in the 4S pack. It follows that the average acceptable deviation in the impedance of the healthy

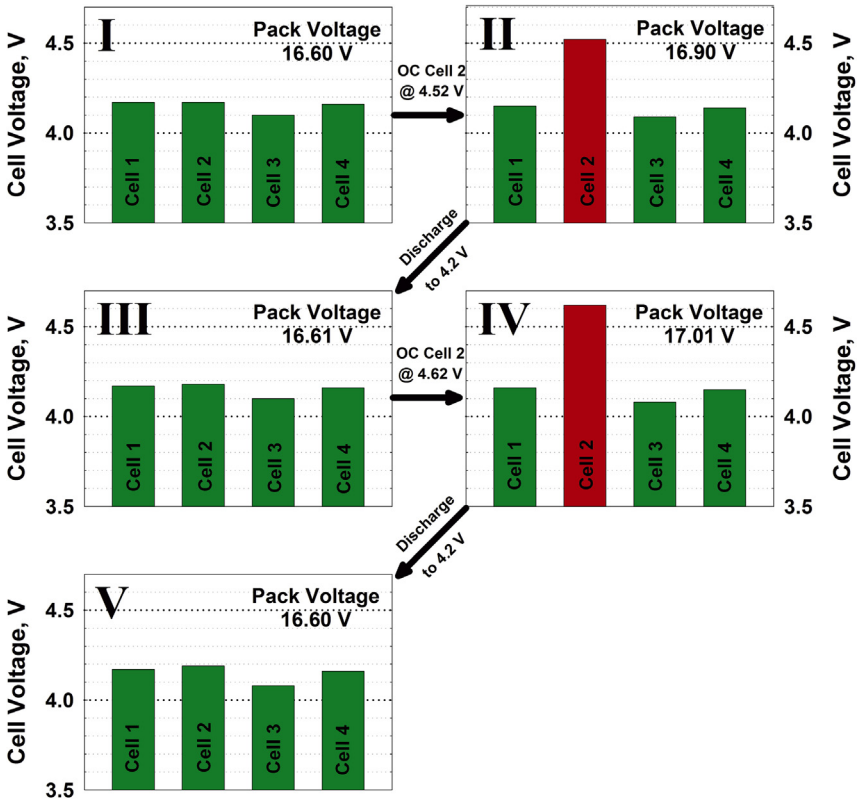

Fig. 8. Individual cell voltages within the 4S pack during direct overcharge (OC) to Cell 2. I. initial 100% SOC condition; II. OC Cell 2–4.52 V (125% SOC); III. discharge Cell 2–4.2 V; IV. OC Cell 2–4.62 V (135% SOC); and V. discharge Cell 2–4.2 V.

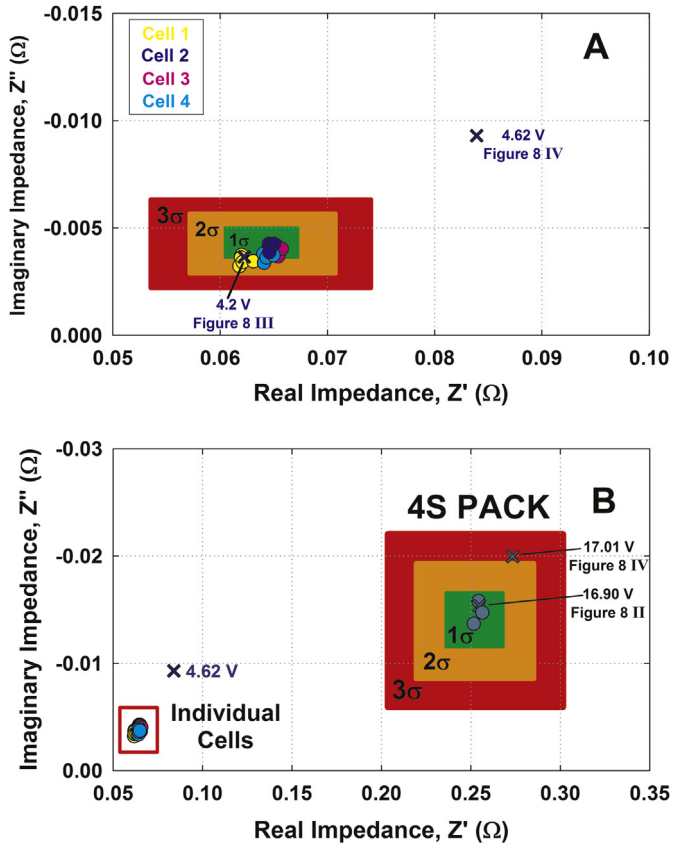

Fig. 9. SOH chart illustrating the impedance at the 316 Hz SOH frequency collected by FlexiMIST for (A) cells 1 through 4. "X" marks denote the overcharge conditions experience by Cell 2 (correlating to I through V in Fig. 8) within the 4S pack and (B) 4S pack impedance encircled by the ±1σ, 2σ and 3σ the standard deviation. "X" marks denote the overall pack voltage associated with overcharges to Cell 2 (correlating to Fig. 8 II and IV).

Table 3
Correlation of Average Impedance Values and Standard Deviation over SOC 100–0% for Individual Cell and 4S Pack using Solartron, Maccor and FlexiMIST Impedance Analysis Instruments.

Individual cells		f_{SOH}	Z′	$\sigma_{Z'}$	Z″	$\sigma_{Z''}$
Solartron	Average of 2 cells	315	.0626	.00147	−.0030	.00076
Maccor	Average of 5 cells	319	.0653	.00341	−.0052	.00043
FlexiMIST	Average of 4 cells	316	.0639	.00348	−.0043	.00072
4S Pack						
FlexiMIST	4S	316	.2524	.0140	−.0168	.00278
FlexiMIST	Sum Cells 1–4	316	.2554	.0139	−.0171	.00287

cells is acceptable, so the packs could probably be increased to 24-V packs (6 cells) or 32-V packs (8 cells) and be effective.

4. Conclusions

A single-point impedance based diagnostic has been applied to monitor state-of-health of lithium ion individual cells and a 4S battery pack. The impedance response at a single perturbation frequency is nearly independent of SOC as determined through routine batch testing cells at various SOC within the safe operating limits of the cell. The 18650 $LiCoO_2$|C cells manufactured by Tenergy show the least variation in impedance response with SOC at a perturbation of 40 mV at f_{SOH} ~316 Hz between 0 and 100% SOC. A SOH range or safety factor of impedance with SOC can be drawn as 1σ, 2σ or 3σ the standard deviation with SOC. Overcharge abuse to individual cells showed variation in the impedance response taken at the SOH frequency well outside of the 3σ SOH region. The single-point diagnostic is able to determine abuse caused by a single cell overcharged +420 mV (135% SOC) above the cutoff voltage in a 4S pack even while the pack voltage remained within the normal operating limits. The single-point technique eliminates the need to collect full impedance spectra and the computational hardware necessary for spectral analysis. The SOH frequency allows for online data collection without a priori knowledge of the SOC and does not require a full charge or discharge cycle prior to collecting the impedance response. The application of this method to other battery systems would depend on the battery-to-battery reproducibility over a much wider range of those samples and the development of detailed statistic on the cell-to-cell impedance variation as a function of temperature and also the integrated system. However these results show that the impedance changes in the 100–500 Hz range are large enough after overcharge abuse to be a valuable indicator of SOH.

Appendix A. Supplementary data

Supplementary data related to this article can be found at http://dx.doi.org/10.1016/j.jpowsour.2014.05.033.

References

[1] Y.-H. Chiang, W.-Y. Sean, J.-C. Ke, J. Power Sources 196 (2011) 3921–3932.
[2] Y. Hu, S. Yurkovich, Y. Guezennec, B.J. Yurkovich, J. Power Sources 196 (2011) 449–457.
[3] B. Wu, V. Yufit, M. Marinescu, G.J. Offer, R.F. Martinez-Botas, N.P. Brandon, J. Power Sources 243 (2013) 544–554.
[4] R. Srinivasan, B.G. Carkhuff, M.H. Butler, A.C. Baisden, Electrochim. Acta 56 (2011) 6198–6204.
[5] R. Srinivasan, B.G. Carkhuff, J. Power Sources 241 (2013) 560–566.
[6] J.P. Schmidt, S. Arnold, A. Loges, D. Werner, T. Wetzel, E. Ivers-Tiffee, J. Power Sources 243 (2013) 110–117.
[7] M. Dubarry, C. Truchot, B.Y. Liaw, J. Power Sources 219 (2012) 204–216.
[8] R. Al Nazer, V. Cattin, P. Granjon, M. Montaru, M. Ranieri, IEEE Trans. Veh. Technol. 62 (2013) 2896–2905.
[9] R. Al-Nazer, V. Cattin, P. Granjon, M. Montaru, M. Ranieri, V. Heiries, in: 27th International Electrical Vehicle Symposium & Exhibition (EVS27), Barcelona, Spain, 2013.
[10] C.T. Love, K. Swider-Lyons, Electrochem. Solid State 15 (2012) A53–A56.
[11] S.S. Zhang, K. Xu, T.R. Jow, J. Power Sources 115 (2003) 137–140.
[12] S. Tobishima, J. Yamaki, J. Power Sources 81 (1999) 882–886.
[13] G. Park, H. Nakamura, Y. Lee, M. Yoshio, J. Power Sources 189 (2009) 602–606.
[14] T. Momma, M. Matsunaga, D. Mukoyama, T. Osaka, J. Power Sources 216 (2012) 304–307.
[15] F.M. Wang, H.Y. Wang, M.H. Yu, Y.J. Hsiao, Y. Tsai, J. Power Sources 196 (2011) 10395–10400.
[16] X.Y. Qiu, Q.C. Zhuang, Q.Q. Zhang, R. Cao, P.Z. Ying, Y.H. Qiang, S.G. Sun, Phys. Chem. Chem. Phys. 14 (2012) 2617–2630.
[17] F. Nobili, F. Croce, B. Scrosati, R. Marassi, Chem. Mat. 13 (2001) 1642–1646.
[18] C. Wang, A.J. Appleby, F.E. Little, J. Electroanal. Chem. 497 (2001) 33–46.
[19] A. Jossen, J. Power Sources 154 (2006) 530–538.
[20] J.P. Schmidt, T. Chrobak, M. Ender, J. Illig, D. Klotz, E. Ivers-Tiffee, J. Power Sources 196 (2011) 5342–5348.
[21] D. Aurbach, J. Power Sources 89 (2000) 206–218.
[22] S. Klink, E. Madej, E. Ventosa, A. Lindner, W. Schuhmann, F. La Mantia, Electrochem. Commun. 22 (2012) 120–123.
[23] G. GirishKumar, W.H. Bailey, B.K. Peterson, W.J. Casteel, J. Electrochem. Soc. 158 (2011) A146–A153.
[24] S.S. Zhang, K. Xu, T.R. Jow, Electrochim. Acta 49 (2004) 1057–1061.
[25] P. Nelson, I. Bloom, K. Amine, G. Henriksen, J. Power Sources 110 (2002) 437–444.
[26] J.N. Reimers, J.R. Dahn, J. Electrochem. Soc. 139 (1992) 2091–2097.
[27] F. Nobili, R. Tossici, R. Marassi, F. Croce, B. Scrosati, J. Phys. Chem. B 106 (2002) 3909–3915.
[28] M. Dubarry, N. Vuillaume, B.Y. Liaw, Int. J. Energy Res. 34 (2010) 216–231.